

Data-driven topology design for conductor layout problem of electromagnetic interference filter

Duanyutian Zhou, Katsuya Nomura, and Shintaro Yamasaki

Abstract—Electromagnetic interference (EMI) filters are used to reduce electromagnetic noise. It is well known that the performance of an EMI filter in reducing electromagnetic noise largely depends on its conductor layout. Therefore, if a conductor layout optimization method with a high degree of freedom is realized, a drastic performance improvement is expected. Although there are a few design methods based on topology optimization for this purpose, these methods have some difficulties originating from topology optimization. In this paper, we therefore propose a conductor layout design method for EMI filters on the basis of data-driven topology design (DDTD), which is a high degree of freedom structural design methodology incorporating a deep generative model and data-driven approach. DDTD was proposed to overcome the intrinsic difficulties of topology optimization, and we consider it suitable for the conductor layout design problem of EMI filters. One significant challenge in applying DDTD to the conductor layout design problem is maintaining the topology of the circuit diagram during the solution search. For this purpose, we propose a simple yet efficient constraint. We further provide numerical examples to confirm the usefulness of the proposed method.

Index Terms—electromagnetic interference filter, topology optimization, deep generative model, data-driven approach

I. INTRODUCTION

IN recent years, noise levels in power electronics circuits have been increasing due to the higher frequencies and faster switching of power devices. Consequently, there is a growing need for high-performance electromagnetic interference (EMI) filters, making it essential to establish effective filter design methods.

In EMI filters, even those with the same circuit topology and components can exhibit different characteristics depending on the conductor layout [1], [2]. This phenomenon is attributed to parasitic elements; specifically, conductor patterns generate equivalent series inductance (ESL), and adjacent conductor patterns form parasitic capacitance [3]. Additionally, magnetic coupling between loops can significantly degrade filter performance in some cases [4]–[6]. The dominant parasitic element varies depending on the circuit topology and parameters, making it challenging to estimate their overall impact. The recent demand for miniaturization and higher density in filters

This work has been submitted to the IEEE for possible publication. Copyright may be transferred without notice, after which this version may no longer be accessible.

Duanyutian Zhou and Shintaro Yamasaki are with the Graduate School of Information, Production and Systems, Waseda University, 2-7 Hibikino, Wakamatsu, Kitakyushu, Fukuoka 808-0135. E-mail: {zhouduanyt2000@ruri, s_yamasaki@waseda.jp}

Katsuya Nomura is with the School of Engineering, Kwansei Gakuin University, 669-1330, 1 Gakuen uegahara, Sanda, Hyogo. E-mail: katsuya.nomura@kwansei.ac.jp

has increased the impact of parasitic effects, further complicating the conductor design of filters. Moreover, international standards for power conversion circuits have been established by the International Electrotechnical Commission (IEC) and the International Special Committee on Radio Interference (CISPR), covering a range from 150 kHz to 30 MHz for conducted noise. There are also standards from 9 kHz to 150 kHz in CISPR 14 and 15 for specific applications [7], [8]. Therefore, it is insufficient to consider only the characteristics at a single frequency; EMI filters must reduce noise over a wide frequency bandwidth. Designing a filter that addresses multiple frequency characteristics while accounting for the effects of complex parasitic elements is a significant challenge, highlighting the need for computer-aided design methods.

Topology optimization is one of the most powerful and effective methodologies to optimize material layout. It was originally proposed in the field of solid mechanics [9]. The basic concept of topology optimization is to replace the original structural (or layout) design problem with a material distribution problem in a given fixed design domain. Usually, the material distribution is represented with nodal or element-wise densities, which indicate material existence with a value from 0 to 1, on the finite element mesh of the discretized design domain. These nodal or element-wise densities are regarded as the design variables, and they are updated towards the optimal material distribution by using mathematical programming with sensitivity information.

Due to the ability of topology optimization to obtain excellent material distributions with a high degree of design freedom, it has recently also become attractive in the field of electromagnetics, for example, in antenna design problems [10], [11], electromagnetic waveguide design problems [12], and in-vehicle reactor design problems [13]. Topology optimization has also been applied to conductor layout design problems of EMI filters [14], [15]. In these works, the objective function is one of the scattering parameters, S_{21} , at a target frequency.

Although optimized conductor layouts were successfully obtained in [14], [15], an approximation method is used in [15] to conduct the electromagnetic analysis for various conductor layouts using a fixed finite element mesh, and approximation errors caused by it are inherently unavoidable. While one does not suffer from such approximation errors when using the conductor layout optimization method proposed in [14], some issues have also been recognized through trials for further developing this method. The first issue is unstable oscillations that occur when the topology of the conductor layout changes. In their methods, the topology of the circuit diagram is preserved because changes to it cause catastrophic

effects on the target EMI filter. On the other hand, topology changes to the conductor layout itself are not prohibited. However, when this occurs, the objective function sometimes significantly degrades, and the conductor material distribution attempts to restore the previous topology in the next iteration of mathematical programming. By repeating these topology changes, unstable oscillations occur. Once the oscillation occurs, the optimal solution search fails.

The second issue is that their methods are not suitable for minimizing S_{21} at multiple target frequencies. This issue is closely related to the first issue because the numerical instability caused by the first issue is amplified when considering two or more target frequencies. The essential reason for these issues is that their methods search for the optimal solution using sensitivity information. In other words, the conductor layout design problem of the EMI filter is essentially strongly nonlinear, and therefore topology optimization is not suitable to solve it.

In order to resolve the essential drawback of topology optimization for strongly nonlinear problems, Yamasaki *et al.* [16] proposed a design methodology called data-driven topology design (DDTD), targeting multi-objective structural design problems. The basic concept of DDTD is the combination of a data-driven approach and a deep generative model, a type of generative artificial intelligence. In DDTD, structures (or layouts) are represented as material distributions in a given design domain, the same as in topology optimization, and elite (high-performance) material distributions are selected from already obtained material distribution data on the basis of the non-dominated rank [17] in the multi-objective function space. Then, the deep generative model learns features of these elite material distributions and generates new material distributions that are diverse but inherit their features. Some of the generated material distributions are expected to have higher performance than the current elite material distributions; therefore, the elite material distributions are updated by selecting from the merged data of the current elite and newly generated material distributions. After that, the updated elite material distributions are used to train the deep generative model again. By repeating these processes, the total performance of the elite material distributions is drastically improved. Thus, DDTD realizes sensitivity-free structural design while maintaining a high degree of freedom for the structural representation.

Although application studies of DDTD have been limited to structural mechanics [16], [18] and fluid dynamics [19], DDTD is considered suitable for the conductor layout design problem of the EMI filter because of its sensitivity-free and multi-objective nature. Therefore, in this paper, we propose a conductor layout design method based on DDTD for minimizing S_{21} at multiple target frequencies.

One significant challenge of this paper is how to maintain the topology of the circuit diagram under the framework of DDTD because this is a specific issue in the conductor layout design of the EMI filter. In previous studies based on topology optimization [14], [15], a constraint using fictitious current and electric field was introduced to maintain the topology of the circuit diagram; however, this constraint is very complicated to implement. Instead, we introduce a simpler and more reason-

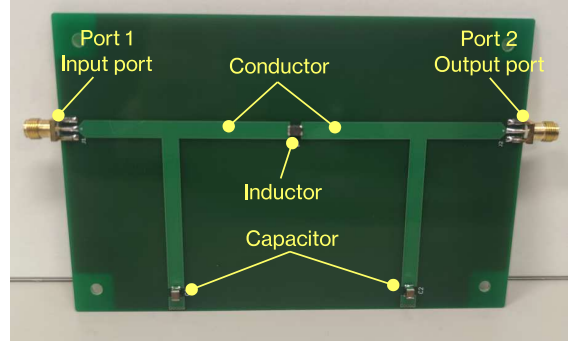


Fig. 1: π -type EMI filter

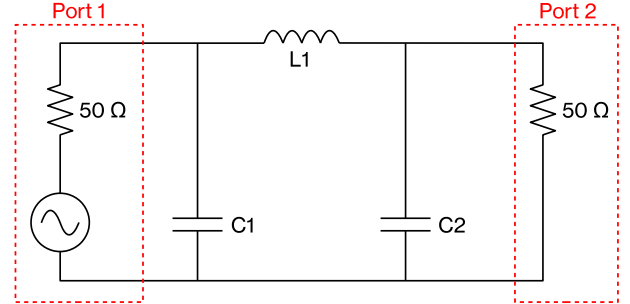


Fig. 2: Circuit diagram of π -type EMI filter

able constraint to preserve it by taking advantage of DDTD. Because DDTD can generate high-performance conductor layouts with a high degree of design freedom, it is expected that we will obtain very complex conductor layouts as the final results. Therefore, considering the physical meanings of the obtained conductor layouts is also an important challenge in this paper.

The rest of the paper is organized as follows. In Section II, we explain a conductor layout design problem of an EMI filter, which is our target in this paper. In Section III, we explain the proposed design method to solve the problem formulated in Section II. In Section IV, we provide numerical examples to demonstrate the usefulness of the proposed method and explore the physical meanings of the obtained results. Finally, we present the conclusion in Section V.

II. CONDUCTOR LAYOUT DESIGN PROBLEM

A. π -type EMI filter

EMI filters block adverse interferences and allow a steady flow of power to protect electronic devices and systems. Their most important function is to reduce electromagnetic noise in a high-frequency range (typically 9 kHz to 30 MHz) while not affecting the passage of current in a low-frequency range (typically 50 Hz or 60 Hz).

Although the noise reduction performance depends on the circuit diagram design and the parameters of the electronic components, different conductor layouts lead to different parasitic effects and capacitive coupling. Therefore, it is also important to find superior conductor layouts for improving noise reduction performance.

There are wide variations of EMI filters. Among them, we select the π -type EMI filter shown in Fig.1 as the target in

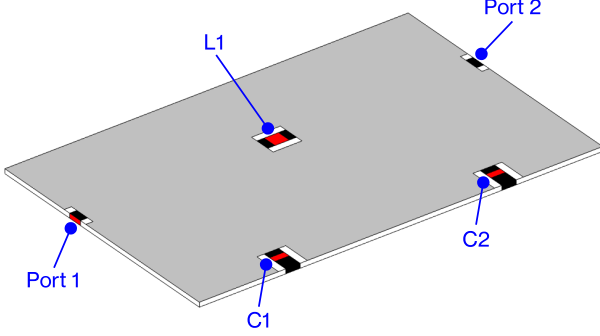


Fig. 3: Computation model of π -type EMI filter

this paper. It has two capacitors and one inductor, as shown in this figure, and these electronic components are connected to the input and output ports using conductors. Figure 2 shows its circuit diagram.

For the π -type EMI filter shown in Figs. 1 and 2, the scattering parameters (so-called S-parameters) can be defined to describe the electrical behavior of the electrical network. Among them, S_{21} represents the transmission coefficient. Therefore, we evaluate the noise reduction performance using S_{21} at target frequencies.

B. Numerical analysis

Figure 3 shows the computation model. Here, the red domains represent ports 1 and 2 (input and output ports, respectively) and the electronic components C1, C2, and L1. The conductor material always exists in the black domains, and it does not exist in the white domains. The back side of the printed circuit board (PCB) is filled with the conductor material. The gray domain is the design domain, in which we consider distributions of the conductor material. In this model, the conductor material is represented as 2D sheets using the impedance boundary condition to account for the skin effect. The scattering boundary condition is imposed on the outer boundaries of the air domain surrounding the PCB.

Similar to [14], we discretize the design domain with a numerical mesh and assign the nodal densities ρ on the mesh. Each component of ρ takes a value from 0 to 1, where 0 means there is no conductor material and 1 means the conductor material exists. We construct the density field ρ , which represents the conductor material distribution, from ρ on the basis of the shape function of the finite element method. Then, we make a body-fitted mesh along the iso-contour of $\rho = 0.5$ for the electromagnetic analysis. By using the body-fitted mesh, we can handle the impedance boundary condition of the conductor material accurately. That is, we use a fixed mesh to represent various conductor material distributions and make a body-fitted mesh for each conductor material distribution when conducting the electromagnetic analysis.

We compute the electromagnetic behavior by solving the governing equations using the finite element method, as introduced in [14]. We also compute S_{21} at target frequencies as explained in that study.

C. Formulation

Although we can consider various conductor material distributions in the design domain, the topology of the circuit diagram in Fig. 2 should be preserved. This is an issue specific to the conductor layout design problem of the EMI filter. In order to resolve this issue, we focus on S_{21} in a low-frequency range. As described above, S_{21} represents the transmission coefficient from port 1 to port 2. Therefore, if the disconnection of the conductor material occurs in the path from port 1 to L1, or from L1 to port 2, S_{21} in a low-frequency range becomes low. On the other hand, if the disconnection of the conductor material occurs between port 1 and C1, or port 2 and C2, S_{21} in a high-frequency range becomes high. Furthermore, if an electrical short bypassing L1 occurs, S_{21} in a high-frequency range becomes high. Therefore, we can preserve the topology of the circuit diagram by minimizing S_{21} in a high-frequency range while keeping S_{21} sufficiently high in a low-frequency range.

On the basis of the above discussion, we formulate the optimization problem to be solved as follows:

$$\begin{aligned} \text{Minimize}_{\rho} \quad & [J_1(\rho), J_2(\rho)] \\ \text{Subject to} \quad & G(\rho) \geq \bar{G}, \\ & 0 \leq \rho_i \leq 1 \quad \text{for } i = 1, 2, \dots, N_{\text{dsg}}, \end{aligned} \quad (1)$$

where

$$\begin{aligned} J_1(\rho) &:= 20 \log_{10} \left| S_{21}^{(f_1)} \right|, \\ J_2(\rho) &:= 20 \log_{10} \left| S_{21}^{(f_2)} \right|, \\ G(\rho) &:= 20 \log_{10} \left| S_{21}^{(f_3)} \right|, \end{aligned} \quad (2)$$

and $S_{21}^{(*)}$ represents S_{21} at a frequency. Frequencies f_1 and f_2 are selected from a high-frequency range, and f_3 is selected from a low-frequency range. As described in (2), we evaluate the decibel values of S_{21} at given target frequencies as the objective and constraint functions $J_1(\rho)$, $J_2(\rho)$, and $G(\rho)$. \bar{G} is the allowable lower bound of $G(\rho)$. In this formulation, we consider ρ as the design variables, where ρ_i is the i -th component of ρ , and N_{dsg} is the number of the design variables.

III. DESIGN METHOD

In this section, we explain the proposed design method to solve the optimization problem formulated in (1).

A. Data process flow

The data process flow of the proposed method is shown in Fig. 4. It starts by providing initial conductor material distributions in some way. In this paper, we introduce a parametric model and provide initial conductor material distributions by randomly changing parameters included in the parametric model. The initial conductor material distributions are treated as the initial data in the form of ρ . The details of the parametric model are explained in Section III-B.

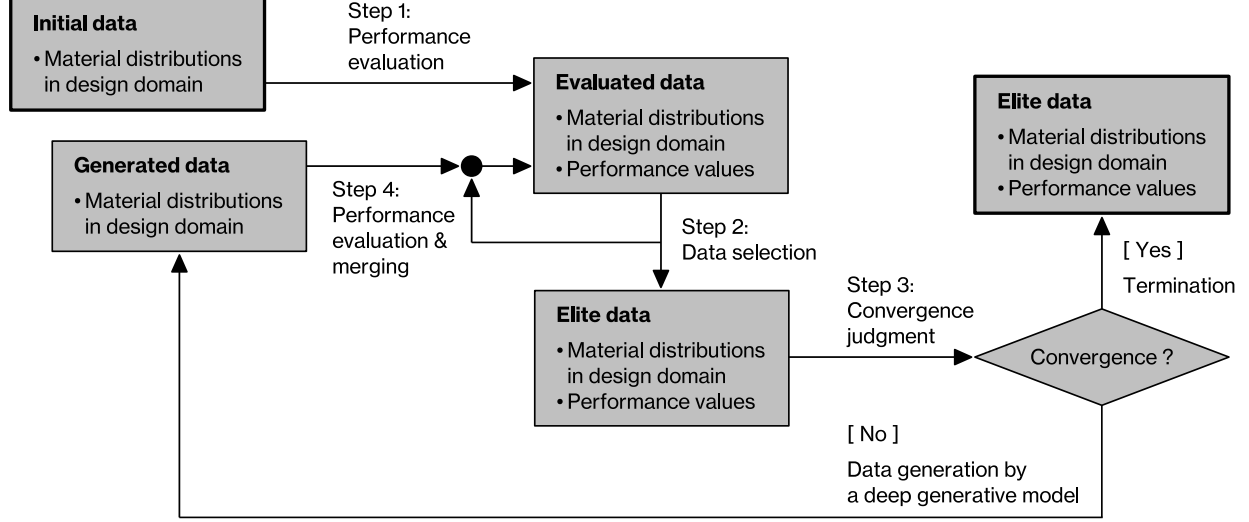


Fig. 4: Data process flow of the proposed method

In step 1, we evaluate the S_{21} values of each conductor material distribution in the initial data using finite element analysis. The conductor material distributions with their performance values are treated as the evaluated data.

In step 2, we calculate the non-dominated rank based on the two objective functions in (1), for the conductor material distributions satisfying the constraint $G(\rho) \geq \bar{G}$. We ignore all the conductor material distributions in the evaluated data that violate the constraint. After that, we select the rank-one conductor material distributions as the elite data. We further copy the elite data and store the copied data for merging in step 4.

In step 3, we check the convergence. If the convergence criterion is satisfied, we output the elite data as the final result. Otherwise, we train a deep generative model using the conductor material distributions of the elite data. Here, we directly use the conductor material distributions in the form of ρ as the training data, in contrast to the previous work [16], where the material distributions are mapped into a regular reference domain before the training. Through the training, features of the training data are learned in a low-dimensional latent space of the deep generative model. Therefore, we generate new conductor material distributions in the form of ρ , which are diverse but inherit features of the training data, by random sampling in the latent space. The generated conductor material distributions are treated as the generated data.

In step 4, we evaluate the S_{21} values of each conductor material distribution in the generated data, similar to step 1, and the generated data with the performance values are merged into the copied elite data in step 2. We update the evaluated data with the merged data and return to step 2.

We iterate these processes until the convergence criterion is satisfied.

B. Parametric model for initial material distributions

Here, we explain the parametric model to provide initial conductor material distributions. This model represents con-

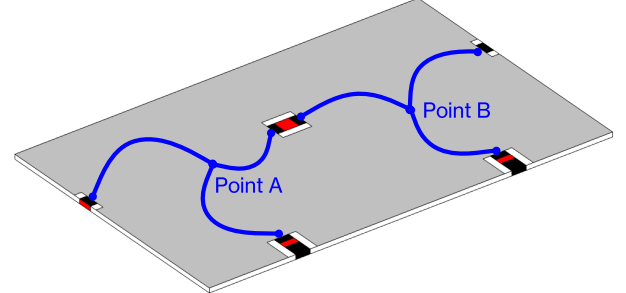


Fig. 5: Parametric model to provide initial conductor material distributions

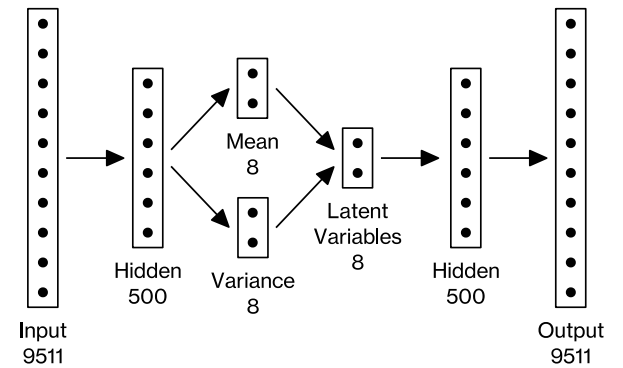


Fig. 6: Network architecture of VAE

ductor material distributions satisfying the topology of the circuit diagram by using six 2nd-order Bézier curves, as shown in Fig. 5. We provide initial conductor material distributions by randomly changing the coordinates of points A and B, and those of the control points of the six Bézier curves. Note that this parametric model is used only for providing initial conductor material distributions, and the above parameters are

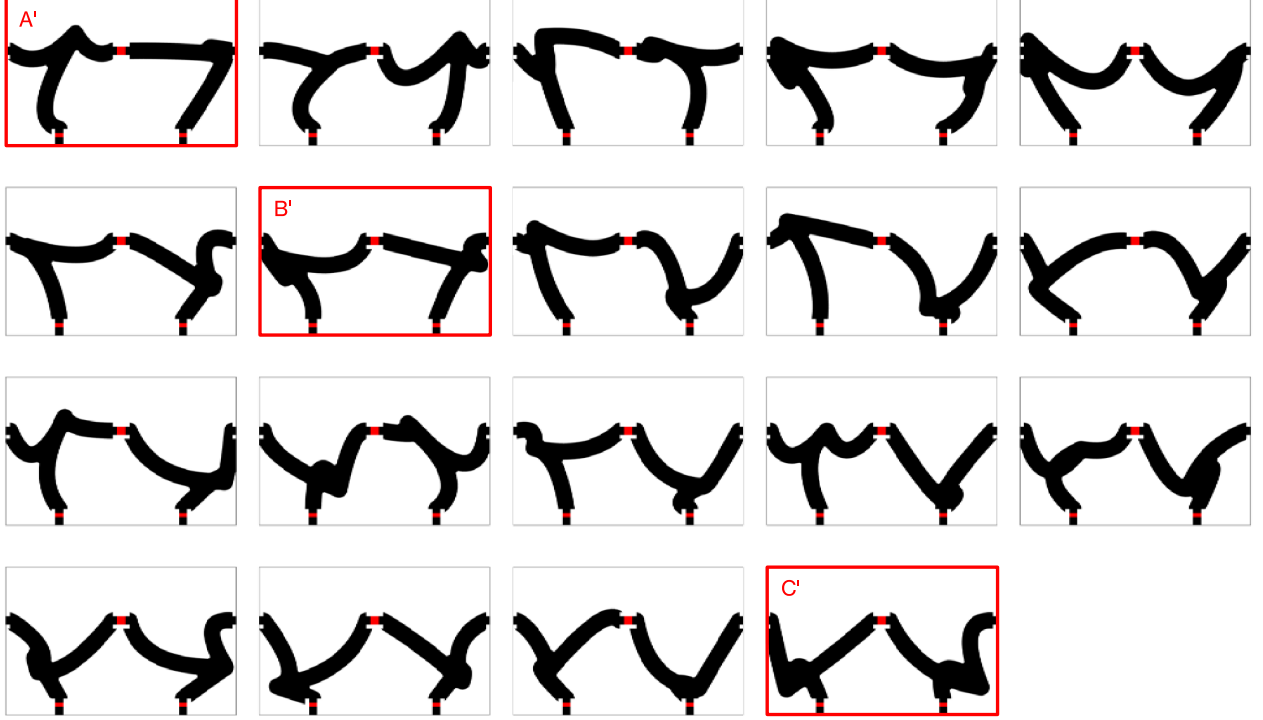


Fig. 7: Elite conductor layouts at iteration 0

not the design variables. The design variables in the proposed method are the nodal densities, as explained in Section II-C.

C. Implementation details

In this section, we explain some implementation details.

For the generative model, we use a variational autoencoder (VAE) whose network architecture is shown in Fig. 6. It is a simple multilayer perceptron-type architecture. The size of the input and output layers, 9511, is the number of the design variables N_{des} in the numerical examples of Section IV. The input layer is fully connected to the hidden layer having 500 neurons. After the ReLU activation, these are fully connected to the 8-dimensional latent space. It is also fully connected to the hidden layer having 500 neurons. After the ReLU activation, these are fully connected to the output layer. Finally, the data are output after the Sigmoid activation.

The loss function of the VAE, L , is given as follows:

$$L := L_{\text{rec}} + \beta \cdot L_{\text{KL}}, \quad (3)$$

where L_{rec} is the reconstruction loss, L_{KL} is the Kullback-Leibler divergence, and β is the weight for L_{KL} . Here, the reconstruction loss is measured by the mean squared error. That is, we use the β -VAE in practice.

For conductor material distributions, it is preferable that ρ_i takes 0 or 1 except in the transition zone with a fixed width. However, it is not ensured for conductor material distributions generated by the VAE. Therefore, we give them this characteristic by using the normalization method proposed in [16].

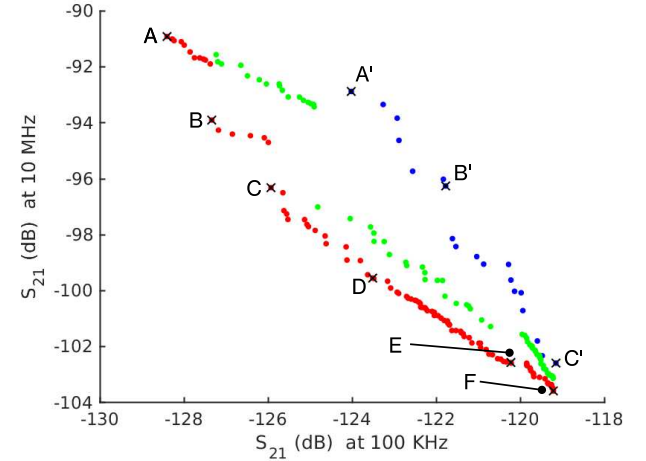


Fig. 8: Performance of elite conductor layouts: iteration 0 (blue), iteration 10 (green) and iteration 70 (red)

IV. NUMERICAL EXAMPLES

In this section, we provide a numerical example to confirm the usefulness of the proposed method. After that, we show what type of conductor material distribution, i.e., conductor layout, is obtained if we don't use the constraint to keep the topology of the circuit diagram. Finally, we consider the reason why the obtained conductor layouts, which are very complex, have high performance from a physics viewpoint.

As explained in Section II, we make a computational model shown in Fig. 3. Here, the size of the PCB is 140 mm \times 90 mm \times 1.6 mm (long side length, short side length, and thickness, respectively), and this PCB is surrounded by the

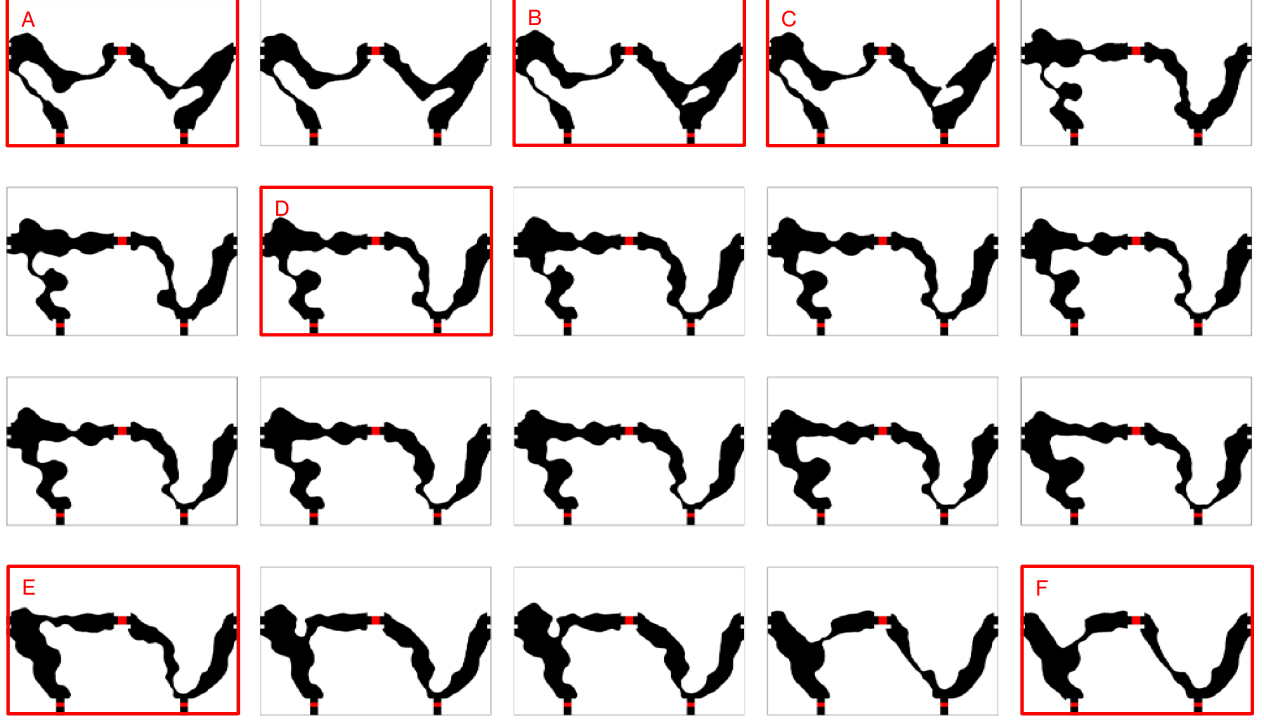


Fig. 9: Elite conductor layouts at iteration 70

air domain whose thickness is 30 mm. The whole analysis domain, including the air domain, is discretized with 367,018 finite elements. The design domain set on the surface of the PCB is also discretized with this finite element mesh, and as a result, the conductor material distribution is represented with 9,511 nodal densities. For the material properties, the relative permittivity of the PCB is 4.5 and that of the air is 1. The relative permeability and electric conductivity are 1 and 1×10^{-8} S/m in the whole analysis domain, respectively.

In this numerical example, we set the target frequencies f_1 and f_2 in (2) as 100 kHz and 10 MHz, respectively. For the constraint to keep the topology of the circuit diagram, we found that the disconnection of the conductor material between ports 1 and 2 can be avoided by ensuring that S_{21} at 1 kHz is greater than or equal to -35 dB through preliminary studies. Therefore, we set f_3 and \tilde{G} to 1 kHz and -35 dB, respectively.

The settings to train the VAE are given as follows: the learning rate is 1.0×10^{-4} , the mini-batch size is 20, the number of epochs is 400, the number of the latent variables is 8, and the weighting coefficient for the KL divergence is 0.5. The sampling in the latent space is done in the same manner as [16]. In addition to the above VAE settings, the maximum number of elite conductor layouts is set to 400. For the convergence criterion of DDTD, we finish the computation of DDTD after 70 iterations. We determined these parameters as a result of preliminary studies.

To conduct the proposed method under these problem settings, we make 100 initial conductor layouts as explained in Section III-B. We then select elite conductor layouts on the basis of the formulation in (1). The number of elite conductor layouts is 19, and these are shown in Fig. 7. Starting from

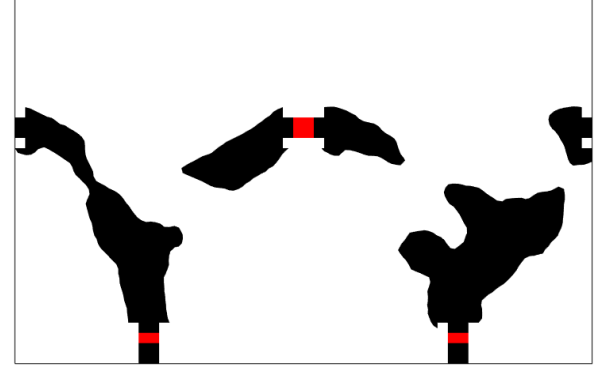


Fig. 10: Elite conductor layout at iteration 1 when deactivating constraint to keep the topology of the circuit diagram

these conductor layouts, the performance of the elite conductor layouts are drastically improved through the DDTD processes, as shown in Fig. 8. The number of finally obtained elite conductor layouts is 103, and some of them are shown in Fig. 9. In Figs. 7 and 8, we select three conductor layouts at iteration 0 and label them as A', B', and C'. Similarly, in Figs. 8 and 9, we select six conductor layouts at iteration 70 and label them as A, B, C, D, E, and F.

Next, we examine the case where the constraint to keep the topology of the circuit diagram is deactivated. Although we use the same initial conductor layouts shown in Fig. 7, we obtain only one elite conductor layout shown in Fig. 10 at iteration 1. Indeed, this conductor layout has excellent performance from the viewpoint of S_{21} at 100 kHz and 10 MHz; these are -208.5 dB and -138.3 dB, respectively. However,

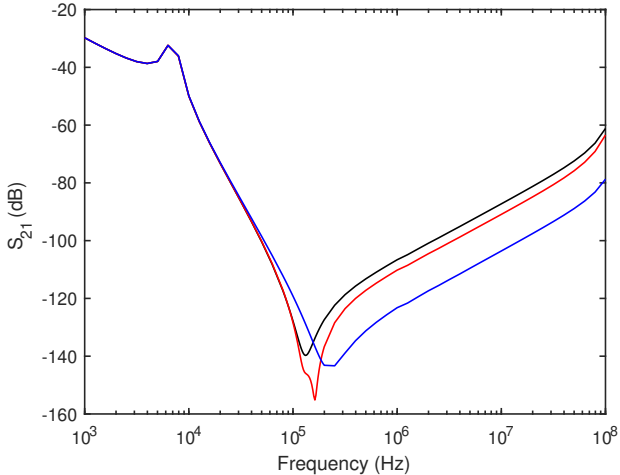


Fig. 11: Frequency response of S_{21} : conductor layout A (red), conductor layout F (blue) and reference conductor layout (black)

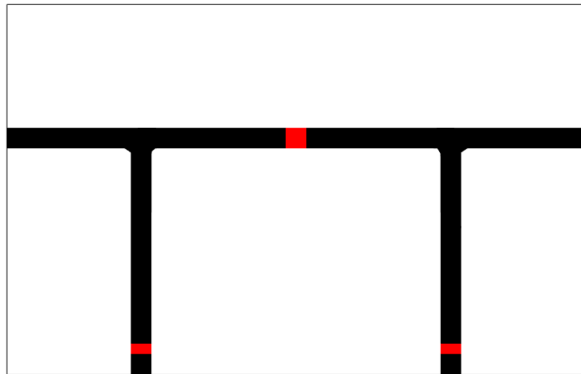


Fig. 12: Simple conductor layout as a reference

such an excellent conductor layout is obviously meaningless because the disconnection of the conductor material occurs between ports 1 and 2. This numerical result indicates that the constraint we introduced is sufficiently effective to keep the topology of the circuit diagram and is essentially needed. Here, we emphasize that our proposed constraint is simple to implement, whereas the constraint proposed in the previous work [14] is complicated. We need only one electromagnetic analysis for the constraint; on the other hand, they need six electromagnetic analyses to keep the circuit diagram topology of the π -type filter in total. This is a significant advantage of the proposed method.

Although the elite conductor layouts at iteration 70 have superior performance as shown in Fig. 8, these layouts are complex as shown in Fig. 9. Therefore, we here consider the physical reasons for the superiority of these complex layouts. Among the 103 layouts at iteration 70, we focus on layout F, which has the smallest S_{21} at 10 MHz, and layout A, which has the smallest S_{21} at 100 kHz. For layouts A and F, we evaluate their S_{21} over a wide frequency range. Figure 11 shows the frequency response of S_{21} for conductor layouts A and F, and also shows that of a conductor layout shown in Fig. 12 as a reference.

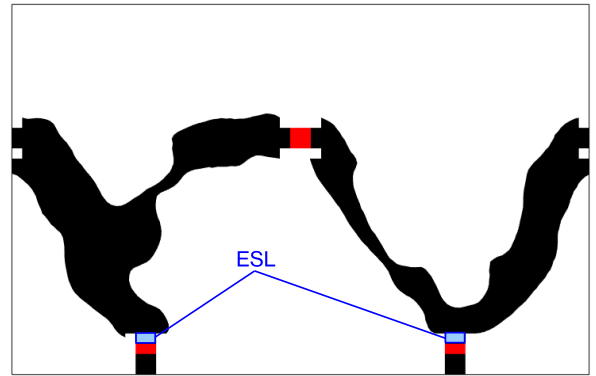


Fig. 13: Inductor insertion on conductor layout F

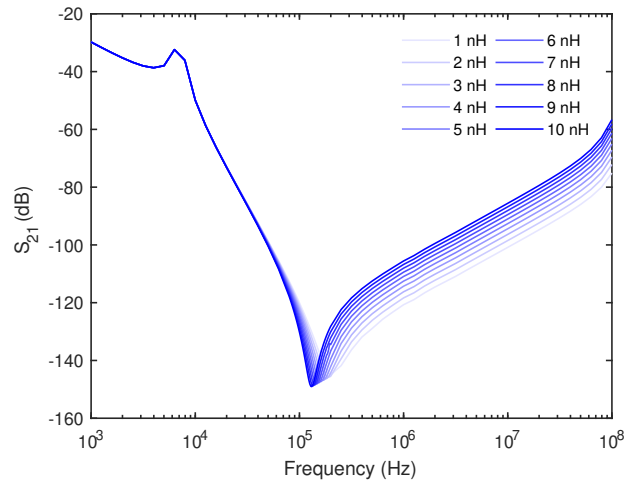


Fig. 14: ESL dependency on S_{21}

First, comparing the performance of conductor layout F with that of the reference conductor layout, the characteristics are greatly improved in the high-frequency range including 10 MHz, but conversely deteriorated at 100 kHz. Looking at conductor layout F, the two branch points have both moved downward compared with the reference conductor layout, and the distance from the branch point to the capacitor has been shortened. This is expected to reduce equivalent series inductance (ESL) and increase the bypass effect, resulting in improved performance in the high-frequency range. To verify this hypothesis, we insert inductors at the position shown in Fig. 13 to check the effect of ESL. The results of the analysis with increasing ESL from 1 nH to 10 nH in 1 nH increments are shown in Fig. 14. As ESL increased, the characteristics in the high-frequency range, including 10 MHz, deteriorated, and furthermore, the characteristics at 100 kHz improved as the resonant frequency decreased with increasing ESL. Therefore, both the performance change of conductor layout F and the trade-off characteristics shown in Fig. 8 were found to be due to ESL.

On the other hand, in Fig. 11, the performance of conductor layout A is slightly improved at high-frequencies, including 10 MHz, and is almost the same at 100 kHz compared to the reference conductor layout. Both responses show a dip due to resonance at a frequency slightly above 100 kHz, and

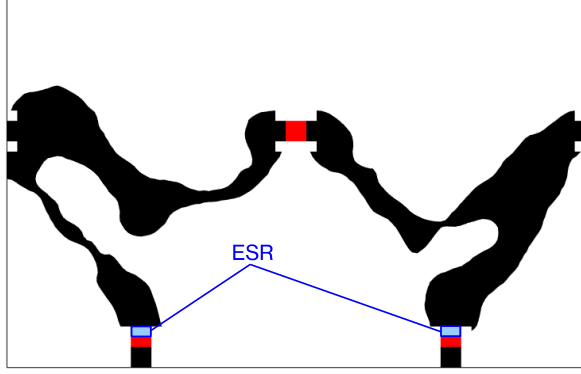


Fig. 15: Resistor insertion on conductor layout A

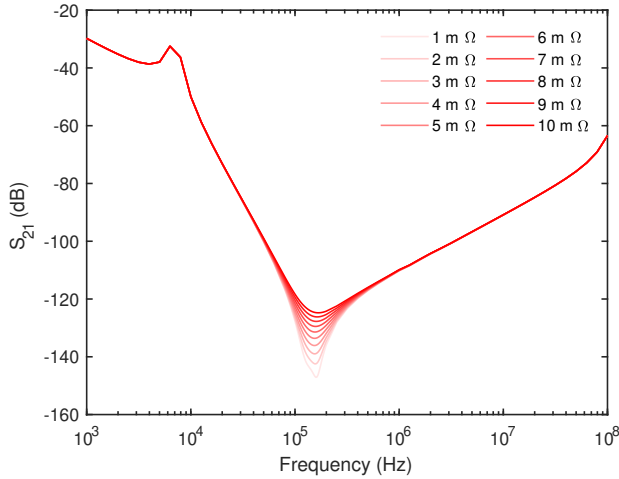


Fig. 16: ESR dependency on S_{21}

the minimum S_{21} value is about -140 dB for the reference conductor layout, while it is less than -150 dB for conductor layout A. We expected this to be due to the lower equivalent series resistance (ESR) at the resonant frequency in conductor layout A. To verify this hypothesis, we inserted resistors at the position shown in Fig. 15 to check the effect of ESR. The results of the analysis with increasing ESR from $1\text{ m}\Omega$ to $10\text{ m}\Omega$ in $1\text{ m}\Omega$ increments are shown in Fig. 16. S_{21} at 100 kHz deteriorates as ESR increases. Thus, it is shown that the performance improvement of conductor layout A can be explained by the reduction of ESR in addition to the reduction of ESL.

V. CONCLUSION

In this paper, we proposed a conductor layout design method based on DDTD for the EMI filter. DDTD is a structural design methodology with a high degree of freedom similar to topology optimization, but in contrast to it, DDTD is sensitivity-free and for multi-objective optimization problems. By leveraging DDTD's nature, we solved a conductor layout design problem for the EMI filter, which is strongly nonlinear and multi-objective. One important task when solving this problem is to maintain the topology of the circuit diagram during the solution search. For this task, we proposed a simple

but efficient constraint based on the S_{21} value in a low-frequency range. Including this constraint, the validity of the proposed method was confirmed using numerical examples. As shown in the numerical examples, the obtained high-performance conductor layouts are very complex compared to a conventional conductor layout as a reference. Therefore, we considered why the obtained conductor layouts are high-performance. As a result, we found that the obtained conductor layouts are substantially effective in reducing ESL and ESR. When considering the practical usage of the EMI filter, S_{21} should be minimized over a given frequency range, not just at a fixed target frequency. Therefore, as future work, we will try to improve the proposed method to minimize S_{21} across an entire given frequency range.

REFERENCES

- [1] S. Wang, F. Lee, D. Chen, and W. G. Odendaal, "Effects of parasitic parameters on EMI filter performance," *IEEE Transactions on Power Electronics*, vol. 19, no. 3, pp. 869–877, 2004.
- [2] S. Wang, Y. Y. Maillet, F. Wang, R. Lai, F. Luo, and D. Boroyevich, "Parasitic effects of grounding paths on common-mode EMI filter's performance in power electronics systems," *IEEE Transactions on Industrial Electronics*, vol. 57, no. 9, pp. 3050–3059, 2009.
- [3] B. Liu, R. Ren, F. F. Wang, D. Costinett, and Z. Zhang, "Capacitive coupling in EMI filters containing T-shaped joint: Mechanism, effects, and mitigation," *IEEE Transactions on Power Electronics*, vol. 35, no. 3, pp. 2534–2547, 2019.
- [4] T. M. Zeeff, T. H. Hubing, T. P. van Doren, and D. Pommerenke, "Analysis of simple two-capacitor low-pass filters," *IEEE Transactions on Electromagnetic Compatibility*, vol. 45, no. 4, pp. 595–601, 2003.
- [5] H. Chen, Z. Qian, Z. Zeng, and C. Wolf, "Modeling of parasitic inductive couplings in a pi-shaped common mode EMI filter," *IEEE Transactions on Electromagnetic Compatibility*, vol. 50, no. 1, pp. 71–79, 2008.
- [6] Y. Murata, K. Takahashi, T. Kanamoto, and M. Kubota, "Analysis of parasitic couplings in EMI filters and coupling reduction methods," *IEEE Transactions on Electromagnetic Compatibility*, vol. 59, no. 6, pp. 1880–1886, 2017.
- [7] A. Ganjavi, H. Rathnayake, F. Zare, D. Kumar, J. Yaghoobi, P. Davari, and A. Abbosh, "Common-mode current prediction and analysis in motor drive systems for the new frequency range of 2–150 kHz," *IEEE Journal of Emerging and Selected Topics in Power Electronics*, vol. 10, no. 1, pp. 74–90, 2020.
- [8] N. N. Esfetanaj, H. Wang, F. Blaabjerg, and P. Davari, "Differential mode noise prediction and analysis in single-phase boost PFC for the new frequency range of 9–150 kHz," *IEEE Journal of Emerging and Selected Topics in Industrial Electronics*, vol. 3, no. 1, pp. 177–187, 2021.
- [9] M. P. Bendsøe and N. Kikuchi, "Generating optimal topologies in structural design using a homogenization method," *Computer Methods in Applied Mechanics and Engineering*, vol. 71, no. 2, pp. 197–224, 1988.
- [10] T. Nomura, K. Sato, K. Taguchi, T. Kashiwa, and S. Nishiwaki, "Structural topology optimization for the design of broadband dielectric resonator antennas using the finite difference time domain technique," *International Journal for Numerical Methods in Engineering*, vol. 71, no. 11, pp. 1261–1296, 2007.
- [11] S. Zhou, W. Li, and Q. Li, "Level-set based topology optimization for electromagnetic dipole antenna design," *Journal of Computational Physics*, vol. 229, no. 19, pp. 6915–6930, 2010.
- [12] S. Yamasaki, T. Nomura, A. Kawamoto, K. Sato, and S. Nishiwaki, "A level set-based topology optimization method targeting metallic waveguide design problems," *International Journal for Numerical Methods in Engineering*, vol. 87, no. 9, pp. 844–868, 2011.
- [13] S. Yamasaki, A. Kawamoto, A. Saito, M. Kuroishi, and K. Fujita, "Grayscale-free topology optimization for electromagnetic design problem of in-vehicle reactor," *Structural and Multidisciplinary Optimization*, vol. 55, no. 3, pp. 1079–1090, 2017.
- [14] K. Nomura, S. Yamasaki, K. Yaji, H. Bo, A. Takahashi, T. Kojima, and K. Fujita, "Topology optimization of conductors in electrical circuit," *Structural and Multidisciplinary Optimization*, vol. 59, no. 6, pp. 2205–2225, 2019.

- [15] K. Nomura, "Density-based topology optimization for conductor design of emi filters with improved impedance boundary condition," in *2022 International Symposium on Electromagnetic Compatibility - EMC Europe*, 2022, pp. 377–382.
- [16] S. Yamasaki, K. Yaji, and K. Fujita, "Data-driven topology design using a deep generative model," *Structural and Multidisciplinary Optimization*, vol. 64, no. 3, pp. 1401–1420, 2021.
- [17] K. Deb, A. Pratap, S. Agarwal, and T. Meyarivan, "A fast and elitist multiobjective genetic algorithm: NSGA-II," *IEEE transactions on evolutionary computation*, vol. 6, no. 2, pp. 182–197, 2002.
- [18] T. Kii, K. Yaji, K. Fujita, Z. Sha, and C. C. Seepersad, "Latent crossover for data-driven multifidelity topology design," *Journal of Mechanical Design*, vol. 146, pp. 051713–1, 2024.
- [19] K. Yaji, S. Yamasaki, and K. Fujita, "Data-driven multifidelity topology design using a deep generative model: Application to forced convection heat transfer problems," *Computer Methods in Applied Mechanics and Engineering*, vol. 388, p. 114284, 2022.